Plasma-induced flow instabilities in atmospheric pressure plasma jets

Amanda M. Lietz,[1,a)] Eric Johnsen,[2,b)] and Mark J. Kushner[3,c)]
[1]Department of Nuclear Engineering and Radiological Sciences, University of Michigan, 2355 Bonisteel Blvd., Ann Arbor, Michigan 48109-2104, USA
[2]Department of Mechanical Engineering, University of Michigan, 2350 Hayward Street, Ann Arbor, Michigan 48109-2125, USA
[3]Department of Electrical Engineering and Computer Science, University of Michigan, 1301 Beal Ave., Ann Arbor, Michigan 48109-2122, USA

(Received 14 July 2017; accepted 27 July 2017; published online 11 September 2017)

Pulsed plasma excitation of rare gases flowing into air has been shown to impact the stability of the flow in non-equilibrium atmospheric pressure plasma jets (APPJs). In this paper, the results from a numerical modeling investigation of the stability of a round He APPJ with a powered electrode exposed to the gas flow are discussed. Localized gas heating at the powered electrode occurs on the time scale of the voltage pulse, tens to 100 ns, which is short compared to the fluid timescales. An acoustic wave propagates from this heated, expanding gas and exits the jet. The wave disturbs the shear layer between the He and surrounding humid air, exciting a shear instability which grows downstream with the flow and increases the mixing of the humid air into the He. The effects of the eddy-dominated flow on ionization wave (IW) propagation in an APPJ were investigated. The IW followed the regions of the highest helium concentration, resulting in an increased production of NO, HO_2, and NO_2. *Published by AIP Publishing*. [http://dx.doi.org/10.1063/1.4996192]

Atmospheric pressure plasma jets (APPJs) have shown promising results as sources of reactive species in biomedical applications including cancer treatment, wound healing, and gene transfection.[1–3] In these plasma sources, a rare gas typically flows through a dielectric tube and into the ambient air, which then diffuses into the rare gas plume. A repetitively pulsed ionization wave (IW) is initiated in the tube. The IW propagates through the rare gas in the tube and into the mixed gas of the plume. Many of the biological responses produced by APPJs are attributed to the production of reactive oxygen and nitrogen species (RONS) by the IW, which mainly occurs at the interface of the rare gas and humid air. Understanding the mixing of the air into the rare gas in the presence of the IW is critical to controlling RONS production. For reproducibility and clarity, most APPJs are intended to operate as laminar jets. However, the propagation of the IW can induce eddies and turbulence in the otherwise laminar flow of the plume,[4,5] increasing the mixing between the rare gas and air, and so affecting the RONS production. Boselli *et al.* reported that an induced turbulent front moved through the plume at approximately the speed of the gas. Schlieren imaging has shown that an instability appears with each voltage pulse and moves at a speed commensurate with the gas flow.[6] In other cases, a naturally turbulent jet can be stabilized by the plasma, particularly when the helium buoyancy opposes the flow.[7]

The onset of the turbulence by IWs in plasma jets has been attributed to one or a combination of electrical or thermal forces. The electrical forces result from the charge separation combined with the large electric field that occurs in the IW passing through the plume. These forces result in a localized momentum transfer from charged species to the bulk fluid flow. The results from the computational investigation discussed in this paper suggest that gas heating by the plasma can be an important stimulus to induce instabilities in the gas flow of typical APPJs.

A round gas jet propagating from a tube into a quiescent fluid is susceptible to instabilities even in the absence of a plasma.[8,9] For jets that are laminar when exiting the tube, these instabilities are first manifested as large unsteady structures at greater than ten L/d (distance from the outlet divided by the diameter of the jet) from the jet outlet. These structures then develop into turbulence at a larger L/d.[10] The Reynolds number for which the jet flow transitions from laminar to turbulent at 10 L/d is approximately 1500.[9] At atmospheric pressure and a tube diameter of 1 mm, this corresponds to a speed of 1.8×10^4 cm/s or flow rate of 8.6 slm. However, this transition strongly depends on the perturbations of the incoming jet flow, and an unsteady flow can develop at lower Reynolds numbers.[10] The critical Reynolds number above which a slot jet is unstable is as small as 4 according to linear stability theory.[11] A more detailed jet stability analysis, which accounts for viscosity, cylindrical symmetry, and an experimental initial velocity profile, was performed by Petersen and Samet.[12]

In this investigation, *nonPDPSIM*, a 2-dimensional plasma hydrodynamic simulation was used to model the plasma, gas dynamics and stability of an atmospheric pressure He plasma jet propagating into humid air. This model was described in detail by Norberg *et al.*[13] The reaction mechanism includes plasma and neutral chemistry for $He/N_2/O_2/H_2O$.[13] The cylindrically symmetric geometry used in this study is shown in Fig. 1. Helium was flowed into the tube at 8 slm with impurities of $N_2/O_2/H_2O = 4.7/2.4/2.9$ ppm. Humid air with a composition $N_2/O_2/H_2O = 79.5/20/0.5$ flowed coaxially around

a)lietz@umich.edu
b)ejohnsen@umich.edu
c)mjkush@umich.edu

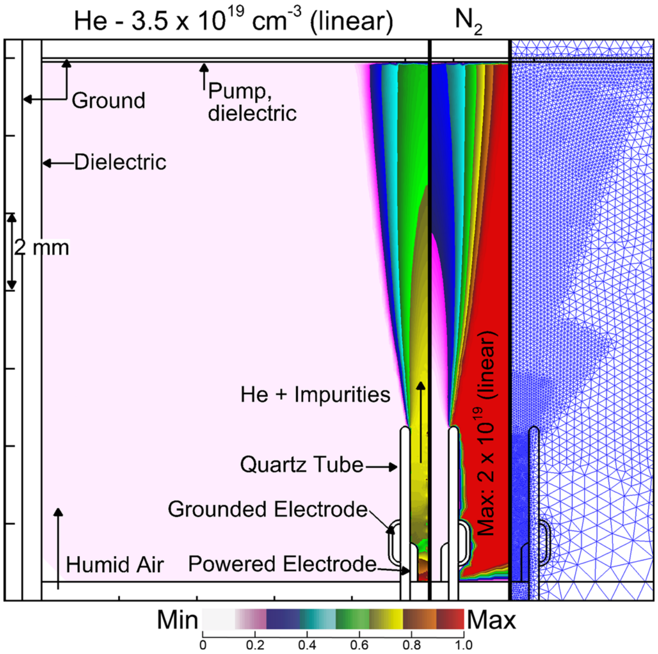

FIG. 1. Cylindrically symmetric geometry used in the model of a plasma jet. The internal electrode is powered and ring electrode is grounded. He and N_2 densities are shown after 5 ms. The mesh contains refinement zones in the tube and spreading radially outward. The mesh spacing is 35 μm in the tube and 90 μm at the pump.

the jet, with a total flow rate of 2 slm over a larger area. The unstructured mesh used in the calculation includes 7089 total nodes and 6011 plasma nodes.

nonPDPSIM includes a fluid dynamics module which solves modified Navier-Stokes equations. A description of the coupling of the calculations of plasma and chemistry to that of the fluid dynamics is in the supplementary material. Although large-scale vortical structures are produced by the algorithms in *nonPDPSIM*, fine scale turbulent dissipation is not represented if occurring on spatial scales smaller than the mesh resolution (67–100 μm in the shear layer). Even if the mesh were fine enough, the 3-dimensional character of the turbulence would not be captured in this 2-dimensional code. This means that *nonPDPSIM* should be considered accurate in determining the source of the flow disturbance, but it should not be considered an exact solution to the long time-scale fluid evolution.

The steady state gas flow field, shown in Fig. 1, was established in 5 ms of computational time before launching the ionization wave. The Reynolds number based on the tube inner diameter is Re = 1250, which produces a stable flow before the voltage pulse is applied. For this essentially laminar flow, as the helium convects out of the tube (average speed of 1.7×10^4 cm/s at the outlet), the ambient air diffuses into the flow, producing the steady state N_2 density shown in Fig. 1. A –14 kV pulse with a 30 ns rise time, a 10 ns fall time and a 50 ns total duration was applied to the annular electrode inside the tube. Poisson's equation and the full plasma dynamics were solved for 70 ns, including 20 ns after the applied voltage returns to zero. After this point, the plasma is assumed to be charge neutral and Poisson's equation is no longer solved. (By this time, the IW has dissipated.) While enforcing charge neutrality, the plasma chemistry and fluid dynamics are then integrated until the end of the simulation, with the electron temperature fixed at $T_e = 0.025$ eV and the electric field set to zero.

The propagation of the IW in this jet begins at the powered electrode and propagates out of the tube, as shown in Fig. 2(a) by the electron impact ionization source. The peak electron temperature in the wavefront of the IW is $T_e = 7.4$ eV. The IW is annular in the tube and adjacent to the wall due to the electric field enhancement that occurs at the inner surface. Outside of the tube, the IW follows the interface between the helium and the ambient air, returning to the axis within 1.3 mm of the tube outlet. These trends are commonly observed in experiments.[14–16] The majority of the RONS production by the IW occurs at the interface between the helium and the air, though some ROS are formed in the tube due to the impurities in the flow (for example, O and OH), as shown in Fig. 2(b). The major production of the RONS at the interface places increased importance on the gas flow dynamics in the mixing layer between the helium and the air.

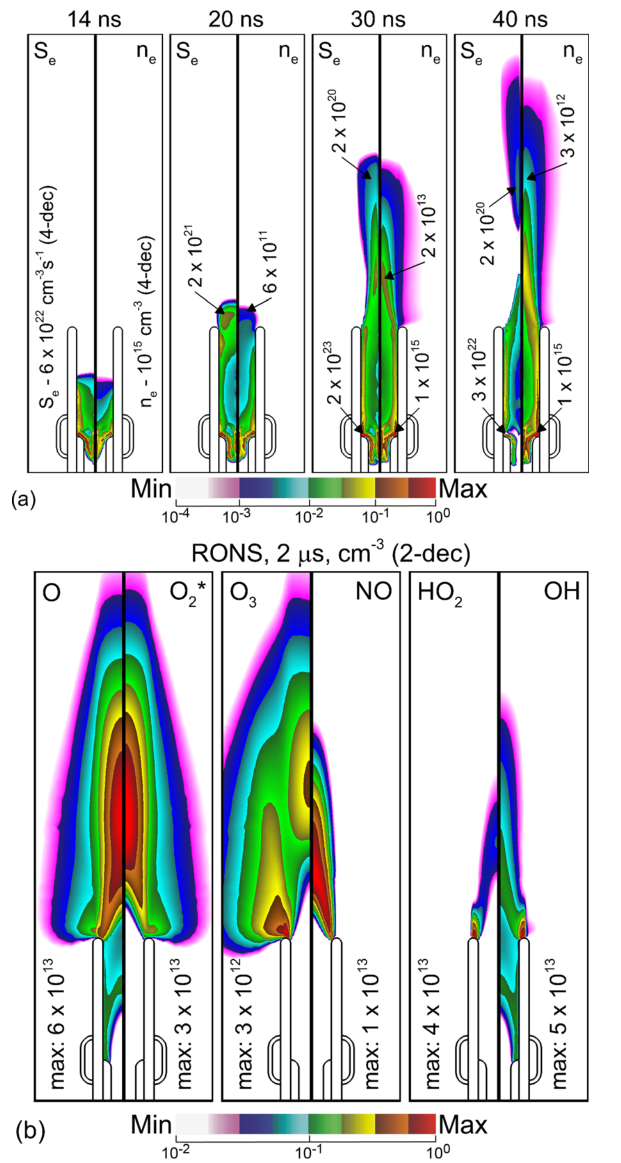

FIG. 2. Plasma properties during and after the IW. (a) Electron impact ionization source (S_e) (left) and electron density (n_e) (right) during the IW, with the maxima indicated (4-decade log scale). (b) The density of RONS at 2 μs after the voltage pulse (2-decade log scale).

There is a region of high electron impact ionization and high electron density surrounding the powered electrode in a cathode-fall like structure. The high electron density and temperature near the surface of the powered electrode produces highly localized energy deposition, resulting in gas heating of $\Delta T_g = 523$ K, as shown in Fig. 3(a), nearly tripling T_g. The plasma-induced gas heating includes Ohmic heating, Frank-Condon heating, and the heating due to exothermic neutral and ion reactions. This heating occurs within a 70 ns pulse, which is nearly instantaneous compared to the fluid timescales ($d/u = 6$ μs, where d is the diameter and u is the flow speed). The end result is a doubling of the pressure in this boundary layer. As this gas expands, a strong acoustic wave propagates along the tube, out into the plume, and into the region of shear flow between the helium and the air. This acoustic wave causes an oscillation in the total number density, which is represented by ΔN_{tot} in Fig. 3(a). The gas cools as it expands, and after 3 μs the gas temperature is 350 K over a much larger volume than the initial region of heating.

To visualize the motion of the interface between the He and the air, ΔN_2 is shown in Fig. 3(a), where ΔN_2 is the current density of N_2 minus the density of N_2 before the voltage pulse. The acoustic wave perturbs this interface and induces a shear instability, as shown in Fig. 3(b). This alternating pattern of increasing and decreasing ΔN_2 is a wave in the interface between the He and air. This wave propagates at the gas flow velocity, which is characteristic of a shear instability and consistent with experimental observations.[5,6] When gas heating was turned off in the model by excluding all forms of heating due to plasma processes, the acoustic wave and instability did not develop (i.e., $\Delta N_{tot} \approx \Delta N_2 \approx 0$). Including or excluding momentum transfer due to charged species did not have a significant effect on the gas flow, and so for these conditions the induced flow instability can be attributed to gas heating.

The flow disturbance produced by the plasma becomes more severe with increasing magnitude of the negative voltage. This trend is consistent with the increase in energy deposition. The disturbance can be quantified by integrating the absolute value of ΔN_2 over the computational domain, and the results of which are shown in Fig. 4. Experimental observations that the onset of turbulence occurs closer to the jet outlet as voltage is increased are consistent with these results.[4,6]

The shear instability produces a disturbance of the gas flow in an important region for the RONS production—the mixing zone. Since much of the RONS of interest for biological applications are produced where the He and humid air merge, the entrainment of air by flow instabilities into the path of the IW can affect the RONS production and the propagation of the subsequent IWs. To demonstrate the effect of this mixing on the behavior of an APPJ, the propagation of an IW into an eddy-dominated flow was simulated, as shown in Fig. 5. The geometry is a slot jet 1 mm wide in Cartesian coordinates, a configuration that produces a less stable flow by allowing the development of asymmetric modes.[8] To approach turbulent conditions, a helium flow of 15 slm/mm and a shroud air flow of 5 slm/mm were used. These conditions correspond to an average He speed at the outlet of 2.5×10^4 cm/s, an average air speed of 430 cm/s, and a Reynolds number of 2380. The simulation produced a pattern of vortex shedding, alternating from each side of the channel. The powered electrode was driven by a –15 kV pulse with a 30 ns rise time, a 10 ns fall, and a total duration of 110 ns. The IW follows the region of the highest He density, curving

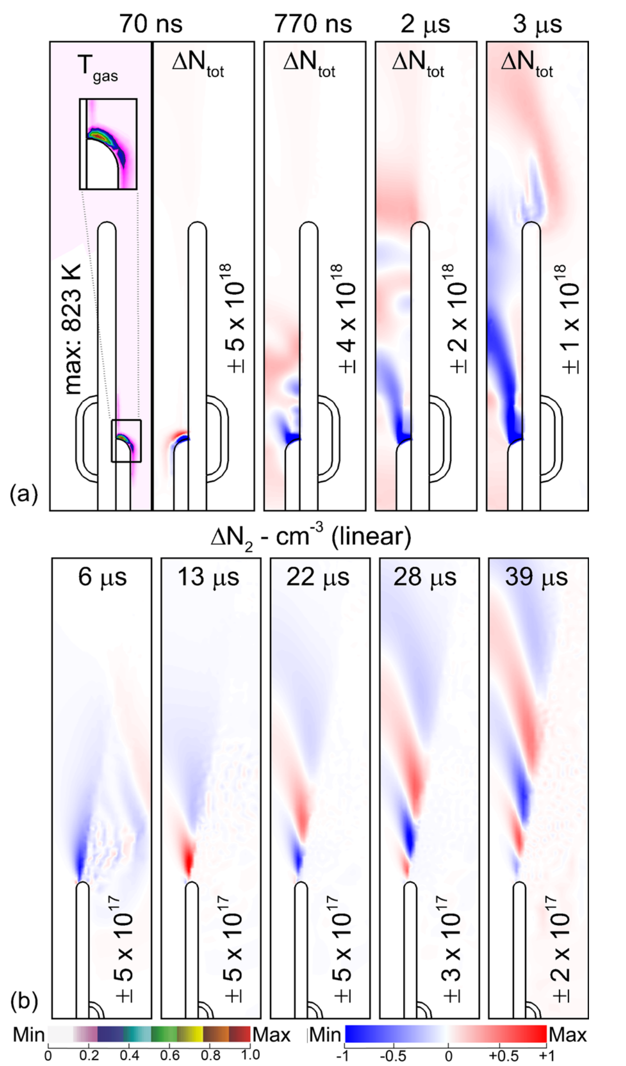

FIG. 3. Plasma produced instabilities. (a) Gas temperature (T_{gas}) at the end of the plasma calculation is shown in the leftmost frame with ΔN_{tot} (the total number density minus the total number density at the start of the voltage pulse). (b) $\Delta N_2 = N_2(t) - N_2(t=0)$ which visualizes the oscillations in the characteristic of a shear instability.

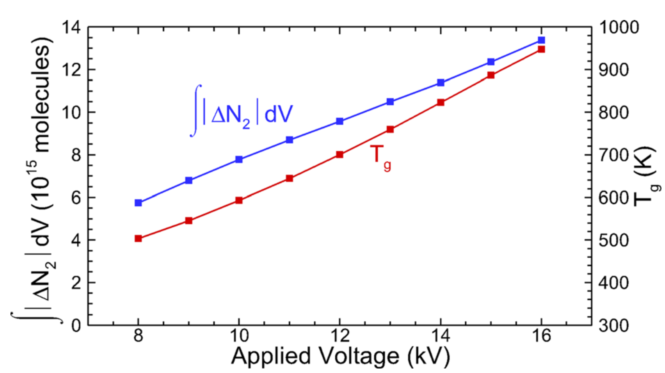

FIG. 4. The plasma-induced fluid disturbance is represented as the absolute value of ΔN_2 integrated over the computational domain where $\Delta N_2 = N_2(t) - N_2(t=0)$. Energy deposition and gas temperature increase with increase in magnitude of negative voltage, which produces a stronger flow disturbance.

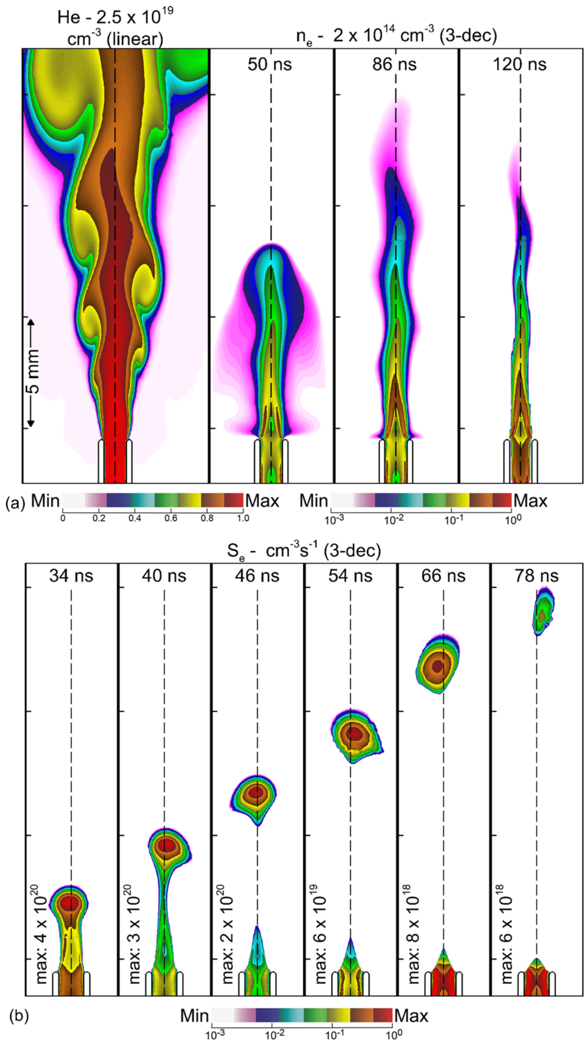

FIG. 5. Characteristics of a slot jet. (a) Initial eddy-dominated helium density for a flow rate of 15 slm/mm, with electron densities as the plasma propagates into the unstable flow. (b) Time evolution of the electron impact ionization source as the IW propagates into the eddy-dominated He plume.

around the eddies where the mole fraction of air is large due to entrainment. The electric field for which the IW can be sustained is lower in He than in air, due to inelastic electron energy loss to low lying vibrational and electronic states, and attachment to O_2 and H_2O. Even in laminar jets, the IW typically terminates at the axial location where the air mole fraction exceeds about 10%.[17] These patterns of the IW following the rare gas flow have been experimentally seen in jets with an eddy-dominated flow.[5,6,17] This manifests itself in the plasma jet appearing "brush-like" as described by Robert *et al.*[18]

To quantify the effects of the eddy-dominated flow on the RONS production, the simulation shown in Fig. 5 was repeated with a He flow of 1 slm/mm which produced a laminar plume. The total inventory of RONS was calculated 2 μs after the beginning of the IW, which dominantly captures the RONS production resulting from the immediate propagation of the IW before advective motion becomes significant. The case with the eddy-dominated flow generally results in more RONS, particularly of more complex species such as HO_2, NO, and NO_2. In the eddy dominated case, the initial inventories of these species increases by factors of 1.5–2.1. The other species examined, O, O_2*, OH, N, and O_3, increase by 10%–27%. These results are sensitive to the past history of the plume, as the previous eddy motion may have aided the transport of humid air into the He plume. As a minimum the eddy-dominated flow provides a larger surface area for the plasma to interact with the humid air and therefore produces more RONS.

In conclusion, the gas flow in an atmospheric pressure plasma jet is fundamentally unstable to a shear instability. In APPJs localized heating at the powered electrode produces an acoustic wave which disturbs the shear layer between the helium and the ambient air. This results in a shear instability, which causes an unsteady flow, and generates a disturbance that propagates with the local gas speed. This could develop into plasma-induced turbulence downstream. Ionization waves propagating into an unsteady plume are influenced by the gas composition profile and follow the region of the highest helium concentration. The result is differences in the type and amount of reactive species which are produced, depending on whether or not the plume is laminar.

See supplementary material for a detailed description of the coupling between the plasma calculation and the fluid dynamic calculation in *nonPDPSIM*.

This work was supported by the Department of Energy Office of Fusion Energy Science (DE-SC000319 and DE-SC0014132), the National Science Foundation (PHY-1519117) and the NSF Graduate Research Fellowship Program.

[1] M. G. Kong, G. Kroesen, G. Morfill, T. Nosenko, T. Shimizu, J. Van Dijk, and J. L. Zimmermann, New J. Phys. **11**, 115012 (2009).
[2] N. Kaushik, N. Uddin, G. B. Sim, Y. J. Hong, K. Y. Baik, C. H. Kim, S. J. Lee, N. K. Kaushik, and E. H. Choi, Nat. Sci. Rep. **5**, 8587 (2015).
[3] S. Sasaki, M. Kanzaki, and T. Kaneko, Appl. Phys. Express **7**, 26202 (2014).
[4] R. D. Whalley and J. L. Walsh, Nat. Sci. Rep. **6**, 31756 (2016).
[5] M. Boselli, V. Colombo, E. Ghedini, M. Gherardi, R. Laurita, A. Liguori, P. Sanibondi, and A. Stancampiano, Plasma Chem. Plasma Process. **34**, 853 (2014).
[6] M. H. Qaisrani, Y. Xian, C. Li, X. Pei, M. Ghasemi, and X. Lu, Phys. Plasmas **23**, 63523 (2016).
[7] E. Robert, T. Darny, S. Dozias, S. Iseni, and J. M. Pouvesle, Phys. Plasmas **22**, 122007 (2015).
[8] S. C. Crow and F. H. Champagne, J. Fluid Mech. **48**, 547 (1971).
[9] T. B. Gohil, A. K. Saha, and K. Muralidhar, Comput. Fluids **64**, 1 (2012).
[10] P. O'Neill, J. Soria, and D. Honnery, Exp. Fluids **36**, 473 (2004).
[11] P. G. Drazin and W. H. Reid, *Hydrodynamic Stability* (Cambridge University Press, 2004).
[12] R. A. Petersen and M. M. Samet, J. Fluid Mech. **194**, 153 (1988).
[13] S. A. Norberg, E. Johnsen, and M. J. Kushner, Plasma Sources Sci. Technol. **24**, 35026 (2015).
[14] D. Maletić, N. Puač, G. Malović, A. Đorđević, and Z. L. Petrović, J. Phys. D. Appl. Phys. **50**, 145202 (2017).
[15] I. Jõgi, R. Talviste, J. Raud, K. Piip, and P. Paris, J. Phys. D. Appl. Phys. **47**, 415202 (2014).
[16] N. Mericam-Bourdet, M. Laroussi, A. Begum, and E. Karakas, J. Phys. D. Appl. Phys. **42**, 55207 (2009).
[17] S. Iseni, A. Schmidt-Bleker, J. Winter, K.-D. Weltmann, and S. Reuter, J. Phys. D. Appl. Phys. **47**, 152001 (2014).
[18] E. Robert, V. Sarron, T. Darny, D. Riès, S. Dozias, J. Fontane, L. Joly, and J.-M. Pouvesle, Plasma Sources Sci. Technol. **23**, 12003 (2014).